Nonorthogonal tight-binding Hamiltonians for defects and interfaces in silicon

Noam Bernstein
Division of Engineering and Applied Sciences, Harvard University, Cambridge, Massachusetts 02138

Efthimios Kaxiras
Division of Engineering and Applied Sciences and Department of Physics, Harvard University, Cambridge, Massachusetts 02138

(Received 22 January 1997; revised manuscript received 18 June 1997)

A computationally efficient and physically accurate method is desirable for simulation of solid-state phenomena that must be modeled by large atomic systems. To this end we present a nonorthogonal tight-binding model Hamiltonian based on the extended Hückel approach. Tests of existing parametrizations of this type of model Hamiltonian on geometries including some low-energy crystal structures, point defects, and surfaces reveal important shortcomings. We develop an improved parametrization and test it extensively on a wide range of crystalline defects and surfaces, and an amorphous sample. Our model is well suited to capture the energetics of crystalline, defective crystalline, and amorphous silicon. [S0163-1829(97)04039-3]

I. INTRODUCTION

Atomistic simulation of solids is becoming increasingly useful in understanding complex processes which involve the dynamics of a large number of atoms, such as bulk and surface diffusion and motion of defects and interfaces. Phenomena such as nucleation and propagation of dislocations, motion of grain boundaries, and the evolution of the amorphous-crystalline interface are examples of systems that require models comprising at least a few hundreds of atoms for realistic description. In the case of covalent solids, the presence of directed and localized bonds produces defect structures that can be significantly different from the equilibrium bulk structure. These cannot be captured easily by phenomenological descriptions, based for instance on continuum models, which makes atomistic simulations all the more relevant and important. A prime example of a covalent solid is silicon, often referred to as the prototypical semiconductor, which has been studied intensively because of its fundamental and technological importance.

There are two conflicting demands on realistic simulations of the types of phenomena mentioned above. The first is the need for accuracy, without which the results of simulations are not meaningful. The second is the need for large system sizes that provide adequate descriptions of the possible variations in the structure. *Ab initio* density-functional theory (DFT) calculations using the local density approximation (LDA) have been shown to be very accurate for semiconductor systems such as silicon. However, these calculations use large bases and include a self-consistent treatment of the electrons, which makes them computationally expensive. Effective interatomic potentials that do not explicitly involve the electronic degrees of freedom allow for very fast computation and make simulations of very large systems (of order millions of atoms) possible. Despite the fact that interatomic potentials for silicon have been studied extensively,[1] their accuracy remains an open question. These potentials miss the fundamental quantum-mechanical nature of the electrons which controls the interatomic bonding, and their validity far from their fitting regime is uncertain. The tight-binding approximation holds the promise of giving a reasonable description of atomic interactions, while being fast enough for molecular-dynamics simulations of relatively large systems. Although the parameters of the tight-binding Hamiltonian must be derived empirically, this approach keeps some of the fundamental physics through a quantum-mechanical description of the electronic degrees of freedom, while the minimal basis and the sparse Hamiltonian make it much faster than DFT/LDA.

Recently, several groups have studied orthogonal[2–5] and nonorthogonal[6,7] formulations of the tight-binding approximation for the description of covalent solids like silicon and carbon. One such formulation assumes that the Hamiltonian and overlap matrices are proportional to each other through the prescription given by extended Hückel theory. The most recent implementation of this formulation for silicon is due to Menon and Subbaswamy.[6] These authors determined the empirical parameters in the Hamiltonian by reproducing the energetics of silicon clusters. Another recent example of a nonorthogonal tight-binding Hamiltonian is the work of Frauenheim *et al.*, who calculate the matrix elements by explicitly computing the appropriate integrals within DFT/LDA, using contracted atomic orbitals.[7]

In this work we present a nonorthogonal tight-binding Hamiltonian for silicon, suitable for the simulation of crystalline and amorphous systems. This model is a modification of the Menon-Subbaswamy approach. We keep the functional form which has few (11) adjustable parameters, and fit the total energies of several structures to *ab initio* results. The structures are chosen to be representative of the geometries found in the crystalline and amorphous systems we are interested in simulating.

The rest of the paper is organized as follows: In Sec. II we describe the functional forms and parameters of the tight-binding Hamiltonian. In Sec. III we compare the results of tests of the various models (those of Menon-Subbaswamy and Frauenheim *et al.* as well as the one introduced here) to DFT/LDA calculations for crystalline defects and surfaces. In the final section we describe the similarities and differences among the Hamiltonians and discuss some observa-

tions on the relationship between the band structure and point defect formation energies, and state our conclusions.

II. MODELS

A. Extended Hückel theory

The foundation of our model is the tight-binding Hamiltonian in the two-center approximation, expressed in a nonorthogonal basis, as described by Menon and Subbaswamy[6] with the modifications noted below[8]. In the following discussion we will denote the tight-binding Hamiltonian from the work of Menon and Subbaswamy as MS-TB, including the choice of parameter values. The tight-binding Hamiltonian which we present in this paper, similar in form to MS-TB but with different parameter values, we will denote as NO-TB (for nonorthogonal tight binding). The basis consists of one s and three p orbitals centered on each atom. Orbitals on the same atom are assumed to be orthogonal to one another because of their symmetry, but orbitals on different atoms are not necessarily orthogonal. The conventional assumption of orthogonal orbitals on neighboring atoms can be shown to be equivalent to a pairwise (classical) repulsion for a particular crystal structure, but the repulsive potential is not necessarily the same for different crystal structures.[9] The computational demands of nonorthogonal and orthogonal tight binding differ only in the additional storage needed for the overlap matrix, and the additional cost of finding the solution and evaluating the forces for the generalized eigenvalue problem rather than the simple eigenvalue problem. For both the memory use and computational cost the differences are only a factor of two, not significant as far as practical computations are concerned. However, this modest increase in the computational expense is offset by the important physics and flexibility added to the model by the nonorthogonal form of the Hamiltonian.

We begin with matrix elements of a hypothetical orthogonal tight-binding Hamiltonian,

$$V_{\lambda\lambda'\mu}(r)=V_{\lambda\lambda'\mu}e^{-\alpha(r-d_0)}C(r), \tag{1}$$

where $V_{\lambda\lambda'\mu}$ is the matrix element for orbitals of type λ and λ' (s or p), μ is the type of overlap configuration (σ or π), and d_0 is the bond length at the experimentally observed equilibrium volume. The functional dependence of $V_{\lambda\lambda'\mu}$ with distance, given in Eq. (1), is the simple exponential used in MS-TB multiplied by the smooth cutoff function $C(r)$,

$$C(r)=\frac{1}{2}\left[1+\cos\left(\frac{\pi(r-R_c)}{W_c}\right)\right], \tag{2}$$

for the purposes of molecular-dynamics simulations. R_c is the radius of the onset of the cutoff and W_c is the width over which the cutoff function smoothly changes from 1 to 0. Extended Hückel theory takes the dependence between the parameters characterizing the elements of the overlap matrix $S_{\lambda\lambda'\mu}$ and the elements of an orthogonal Hamiltonian $V_{\lambda\lambda'\mu}$ to be

$$S_{\lambda\lambda'\mu}=\frac{2V_{\lambda\lambda'\mu}}{K(r)(\epsilon_\lambda+\epsilon_{\lambda'})}. \tag{3}$$

$K(r)$ is the Hückel nonorthogonality coefficient, which in this work, as in MS-TB, varies with the distance between the two atoms as

$$K(r)=K_0+C_0(r-d_{\min})^2. \tag{4}$$

In the MS-TB model the parameters that govern the variation with distance and the position of the minimum, C_0 and $d_{\min}$, are fixed to be equal to α and d_0, respectively. Since there is no physical rationale for this assumption, we let C_0 and $d_{\min}$ vary independently. ϵ_λ is the energy eigenvalue of an orbital of type λ (s or p). The parameters $S_{\lambda\lambda'\mu}$ and $V_{\lambda\lambda'\mu}$ and geometrical factors determine the elements of the matrices S_{ij} and V_{ij}, as discussed in Harrison.[9] The corresponding relation for the Hamiltonian matrix elements H_{ij} (expressed in the nonorthogonal basis) as a function of the hypothetical orthogonal matrix elements V_{ij} is

$$H_{ij}=\left(1+\frac{1}{K_{ij}}-S_{2_{ij}}^2\right)V_{ij}. \tag{5}$$

The function

$$S_2(r)=\frac{S_{ss\sigma}(r)-2\sqrt{3}S_{sp\sigma}(r)-3S_{pp\sigma}(r)}{4} \tag{6}$$

describes the overlap between two sp^3 hybrids, with an implicit distance dependence through the $S_{\lambda\lambda'\mu}$ terms. Correcting an erroneous term in the MS-TB expression, we use Harrison's original derivation for S_2 which does not include a $V_{pp\pi}$ term.[9]

The eigenvalues of the generalized eigensystem

$$H\psi_n=\epsilon_n S\psi_n \tag{7}$$

are the single particle states. These contribute to the total energy through a band-structure term. The other contribution to the total energy is a classical pair repulsion given by

$$V_{\rm rep}(r)=\chi_0 e^{-4\alpha(r-d_0)}. \tag{8}$$

After fitting the model parameters, we find that this last term, as in the MS-TB model, is extremely small. In orthogonal tight-binding schemes the (screened) Coulomb repulsion of the cores and the nonorthogonality of the real s and p orbitals both contribute to the effective classical repulsion. Apparently, this repulsion is greatly reduced in our model because we explicitly include the nonorthogonality of the orbitals. The total energy is given by

$$E_{\rm tot}=\sum_{\rm occ\ n}\epsilon_n+\sum_{\langle ij\rangle}V_{\rm rep}(r_{ij}) \tag{9}$$

and the corresponding force on atom i is

$$\vec{F}_i=-\sum_{\rm occ\ n}\left\langle\psi_n\left|\frac{\partial H}{\partial\vec{r}_i}-\epsilon_n\frac{\partial S}{\partial\vec{r}_i}\right|\psi_n\right\rangle-\sum_j\frac{\partial V_{\rm rep}(r_{ij})}{\partial\vec{r}_{ij}}. \tag{10}$$

The three parameters which are not subject to fitting are $d_0=2.35$ Å, $R_c=4.027$ Å, and $W_c=1.0$ Å. The first is sim-

ply a scaling factor, chosen for convenience to be the nearest neighbor distance at equilibrium in the diamond structure. The latter two are chosen so that the active region of the cutoff function $C(r)$ does not overlap with any neighbor shells in the diamond structure, and so that the range of $C(r)$ is the same as the range of the matrix elements in the model proposed by Frauenheim *et al.* (see the next subsection). The remaining parameters that enter in the definition of this model Hamiltonian are determined by fitting to a dataset of *ab initio* total energy calculations as discussed in Sec. III.

B. Density-functional tight binding

The Hamiltonian proposed by Frauenheim and coworkers is also a tight-binding Hamiltonian in the two-center approximation, with a nonorthogonal sp^3 basis.[7] All of the matrix elements are computed by explicit evaluation of the appropriate integrals, such as $S_{ij}=\langle\phi_i|\phi_j\rangle$ and $H_{ij}=\langle\phi_i|H|\phi_j\rangle$. The $|\phi_i\rangle$ are eigenfunctions from DFT/LDA calculations of a single atom in a confining potential. The classical repulsion term is obtained by fitting the cohesive energy curves of the silicon dimer and bulk silicon in the diamond lattice structure to DFT/LDA calculations. In the following discussion we will denote this Hamiltonian as DF-TB (density-functional tight binding). While this is an appealing formulation, it may be somewhat restrictive. It is not clear that the matrix elements, calculated using contracted DFT/LDA wave functions of isolated atoms, can be used in any environment without any fitting. As will be discussed in the following section, the performance of this Hamiltonian in some of the geometries we tested is not satisfactory.

We attempted to improve on this formulation by keeping certain features of the model and introducing some fitting parameters to increase its transferability. Since one of the most uncertain aspects of tight-binding Hamiltonians is the distance dependence of the matrix elements, we found it useful to adopt this particular feature from the DF-TB model but allow the magnitude of the matrix elements to vary. However, our attempts at fitting a tight-binding model with this distance dependence to a total energy dataset failed to give a significant improvement. For this reason we do not provide here a new parametrization of the DF-TB model, although we compare its predictions to those of the other two model Hamiltonians studied.

III. FITTING AND TESTS

To determine the values of the parameters for the NO-TB Hamiltonian we fit some results of the model to an *ab initio* dataset, which includes information about bulk structures and point defects. For bulk properties of silicon, we include the total energy as a function of volume for the diamond and β-Sn structures (the two lowest energy, experimentally observed structures of silicon) and the experimental indirect band gap of the diamond structure. The energetics of point defects included in the dataset are the formation energies of the vacancy and two kinds of self-interstitials, and the energy barrier for the concerted-exchange mechanism for diffusion.[10] Interstitials and vacancies are the dominant point defects seen in crystalline silicon, and their formation and migration energies control solid-state processes such as bulk diffusion.[11] Concerted exchange is a theoretically proposed mechanism for diffusion without involving vacancies or interstitials.[10] The saddle-point configuration of the concerted-exchange path includes two broken bonds relative to the ideal crystal, leading to a substantial activation energy (4.5 eV). The usual defect mechanisms, where the activated states correspond to bond breaking in highly distorted environments, have considerably lower activation energies for migration (a low as a few tenths of an eV), and represent a different aspect of atomic processes in Si. All the above structures are chosen to describe the type of geometries expected to be encountered in simulations of crystalline and amorphous silicon. The atoms in these structures are primarily fourfold coordinated, with some distortion of the bond angle and length, as well as some threefold and fivefold coordinated atoms. The formation energies and energy barriers which govern the kinetics of solid-state processes, dominated by bond breaking and healing both in distorted (e.g., point defects) and in undistorted environments (e.g., the concerted exchange), should be reasonably close to the range of energies discussed here.

TABLE I. Parameters in the NO-TB and MS-TB Hamiltonians: the former were generated by fitting to the *ab initio* total energy dataset described in the text. ϵ_s and ϵ_p are the on-site energies for the s and p orbitals, respectively. $V_{\lambda\lambda'\mu}$ are the magnitudes of the matrix elements $V_{\lambda\lambda'\mu}(r)$ at $r=d_0$, and α is the decay length in the exponential distance dependence of the matrix elements [see Eq. (1)]. $d_{\min}$ is the position of the minimum of the parabola in the expression for $K(r)$ [see Eq. (4)]. K_0 and C_0 are the magnitude of $K(r)$ at $r=d_{\min}$ and the curvature of the parabola as a function of r, respectively. χ_0 is the magnitude of the classical repulsion function $\chi(r)$ at $r=d_0$ [see Eq. (8)].

	NO-TB	MS-TB
ϵ_s (eV)	-13.10	-13.55
ϵ_p (eV)	-5.85	-6.52
$V_{ss\sigma}$ (eV)	-1.82	-2.37
$V_{sp\sigma}$ (eV)	1.66	2.52
$V_{pp\sigma}$ (eV)	3.09	3.32
$V_{pp\pi}$ (eV)	-0.58	-1.07
α (Å^{-1})	1.726	1.6
$d_{\min}$ (Å)	2.255	2.36
K_0	1.420	1.7
C_0	1.965	1.6
χ_0 (eV)	0.00822	0.05

The parameters which result from this fitting are listed in Table I. We emphasize that, as will be discussed below, the fit to the dataset is not perfect. The very complex functional forms of the models result in a difficult optimization problem, in which parameters need to be found that minimize deviation from the the energies of the structures included in the dataset. We use a simulated annealing procedure to accomplish this task. However, due to the complexity of the problem, this can only be viewed as getting close to a reasonable set of parameters, while a perfect match to targeted values is rather difficult, if at all possible.

We also performed additional tests of the model Hamiltonians, by considering a range of structures beyond the ones

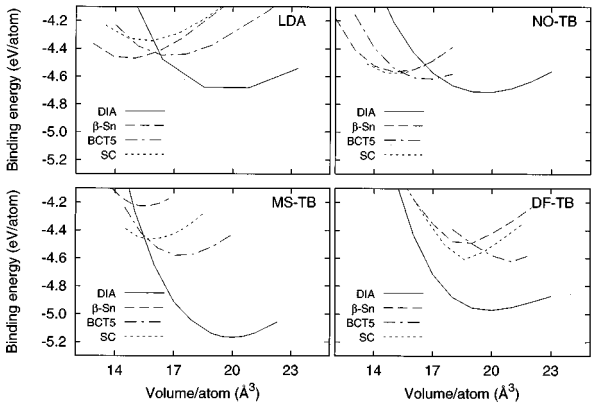

FIG. 1. Cohesive energy curves for the diamond structure (DIA), β-Sn, body-centered-tetragonal-5 (BCT5), and simple-cubic (SC) lattices from four different calculations (DFT/LDA, NO-TB, MS-TB, and DF-TB).

included in the fitting dataset. These comprise more low-energy bulk lattices, as well as relaxed structures for each point defect and the relaxed structure of the concerted-exchange saddle point. The surface energies for several reconstructions of the (100) and (111) surfaces were also examined as part of the testing. The comparison to surfaces provides a sensitive test of how reliable the model Hamiltonians are, since the atomic geometries on surfaces are significantly different from those in the fitting dataset. In the following, results from the fitting and testing calculations with DFT/LDA, DF-TB, MS-TB, and NO-TB are compared.

A. Bulk lattices

The results for the total energy as a function of volume for various low-energy silicon structures are plotted in Fig. 1. The diamond structure, with its fourfold coordination and sp^3 bonding, is the ground state. The β-Sn structure is a low-energy sixfold coordinated structure observed experimentally under high pressure.[12,13] It has also been extensively studied using DFT/LDA.[14–16] The accuracy of NO-TB in reproducing the energetics of these structures is important in establishing its reliability. As is apparent from the graph, NO-TB agrees very well with DFT/LDA calculations for the diamond and β-Sn structures of silicon. The agreement is substantially better than the other two models, as expected since these two structures were included in the fitting dataset of the present model. Our model does, however, overestimate the binding energy for the other structures examined, a body-centered-tetragonal structure with fivefold coordination proposed by Boyer *et al.*[15] (BCT5) and simple cubic (SC). These are both low-energy structures for silicon with relatively low coordination numbers (5 for BCT5 and 6 for SC). Higher coordination bulk phases of silicon (such as bcc, fcc, hcp, etc.) are usually not relevant experimentally because of their high energy.

The Hamiltonian we present here also gives a more accurate bulk modulus than earlier tight-binding models, as can be seen in the tabulated results obtained from fitting the Birch-Murnaghan equation of state[17] to the energy-versus-volume curves (Table II). An additional sensitive test is provided by other elastic constants for the diamond structure, which are listed in Table III. The MS-TB and NO-TB models differ substantially, the latter predicting softer elastic constants closer to the DFT/LDA calculations,[18,19] with errors of 12–33 %. The results of the DF-TB are more accurate than either MS-TB or NO-TB for the bulk elastic constants.

TABLE II. Bulk properties of various crystal lattices. The DFT/LDA cohesive energy numbers are shifted uniformly so that the value for the diamond structure matches the experimental result.

Structure	DFT/LDA	NO-TB	MS-TB	DF-TB
		Binding energy (eV/atom)		
diamond	-4.70	-4.71	-5.19	-4.97
β-Sn	-4.47	-4.57	-4.27	-4.48
BCT5	-4.45	-4.62	-4.64	-4.62
SC	-4.35	-4.58	-4.50	-4.58
		Equilibrium volume (Å^3/atom)		
diamond	19.67	19.67	19.98	19.87
β-Sn	14.63	15.16	15.70	18.67
BCT5	16.77	16.67	17.17	20.98
SC	15.44	15.02	15.63	18.99
		Bulk modulus (GPa)		
diamond	98.0	104.8	153.5	115.1
β-Sn	129.1	138.1	164.7	190.5
BCT5	111.4	134.6	163.3	265.5
SC	117.3	147.5	182.0	244.7

Since the emphasis here is on reproducing total energies accurately, we have not placed much attention in fitting the band structure. Nevertheless we have made an effort to ensure that key features of the band structure, like the valence bandwidth and the band gap are reasonably accurate. A comparison of these features for the three Hamiltonians considered here is given in Table IV.

B. Point defects

Point defects are commonly seen even in the best prepared silicon crystal and are responsible for important processes such as diffusion. Accordingly, an accurate reproduction of their energetics is important for simulations of solid-state systems. The formation energies, E_f, for three representative point defects as obtained from the various model Hamiltonians considered and from DFT/LDA calculations, which were included in the fitting dataset, are listed

TABLE III. Elastic constants of the diamond lattice structure. c_{44}^* is the value of the elastic constant without including the relaxation of the atomic basis.

	DFT/LDA [a]	NO-TB	MS-TB	DF-TB
c_{11} (GPa)	166	145	218	185
c_{12} (GPa)	63.3	84.5	121	80.1
c_{44}^* (GPa)		135	162	135
c_{44} (GPa)	79.3	53.4	81.6	89.5

[a]From Ref. 19.

TABLE IV. Band structure features for diamond structure silicon. The DFT/LDA results include a 0.6-eV scissor-operator shift of the conduction levels (Refs. 20 and 21).

	DFT/LDA	NO-TB	MS-TB	DF-TB
Valence band width	11.92	11.75	13.83	10.69
Band gap at Γ	3.15	1.68	3.07	3.20
Minimum band gap	1.14	1.51	2.72	3.20
Minimum band and gap location	3/4 X	L	L	Γ

in Table V. We considered the self-interstitial in the tetrahedral and hexagonal configurations, and the vacancy. All of the defect calculations were performed in a 216 atom cubic diamond structure supercell with one atom added to, or removed from, the ideal configuration. Due to the large volume of the unit cell, k-point sampling was restricted to the Γ point only.

For the interstitial defects, while the lowest-energy configuration is believed to be a split interstitial, the configurations we considered have the advantage of being conceptually simple and easy to define and visualize. They may also be important stationary points in the path of a diffusing interstitial atom (local minima, i.e., metastable, or local maxima, i.e., saddle points).[23] The objective here is to determine the accuracy with which the model Hamiltonians represent the energetics of a given plausible atomic configuration. The tetrahedral interstitial is a high-symmetry, low-energy configuration. It has four nearest neighbors to which it attempts to form sp^3 bonds. The four neighbors of the tetrahedral interstitial are fivefold coordinated, having as neighbors four crystal atoms and the interstitial. Although it is more difficult to define an interstitial position in an amorphous system, overcoordinated atoms (or floating bonds[24]) analogous to the neighbors of an interstitial can occur,[25] and a realistic representation of this geometry is important for simulating the amorphous system. The hexagonal interstitial is also a high-symmetry, low-energy configuration, although at least in the unrelaxed geometry it is higher in energy than the tetrahedral interstitial. It is positioned in the center of a hexagonal ring in the diamond structure. This position is half way between two adjacent tetrahedral interstitial positions, and can be viewed as the saddle point for diffusion of interstitial atoms between tetrahedral positions. Since the kinetics of activated processes (such as diffusion of interstitials) is controlled by the energy of the transition states, accurate calculation of such potential saddle-points structures is important. The saddle-point configurations of the vacancy and the concerted exchanged were also considered in fully relaxed geometries.

Both the MS-TB and DF-TB Hamiltonians overestimate the formation energies of the self-interstitials by factors of two to three as compared with DFT/LDA. These large errors indicate potential problems in simulating bulk systems with bonding geometries similar to these defects, including crystalline silicon where these defects are often seen, and amorphous silicon where overcoordinated atoms are present. This exemplifies the problems associated with using semiempirical models such as tight-binding Hamiltonians in environments where they have not been fit or adequately tested. The NO-TB model Hamiltonian includes these defects in the fitting dataset, and consequently is much more accurate than either the MS-TB or DF-TB models.

The vacancy is a different type of low-energy point defect seen in crystalline silicon. Undercoordinated atoms (or dangling bonds[24]), similar to those surrounding the missing atom in the crystal vacancy, are also observed in amorphous samples.[25] As in the case of the interstitials, the MS-TB Hamiltonian overestimates the formation energy of the vacancy as compared with our DFT/LDA calculations. The DF-TB Hamiltonian, on the other hand, gives more realistic values for the vacancy formation energy. This indicates that there are qualitatively different properties to under- and overcoordinated point defects, and both need to be checked to ensure the reliability of a particular model. The parameters of the NO-TB Hamiltonian improve the vacancy formation energy as compared to the MS-TB model, reducing the error to less than 1 eV.

As a further test of the accuracy of these Hamiltonians, each was used to relax the three point defects with a conjugate-gradient energy minimization algorithm. Except as noted below, we do not apply any constraints to fix the symmetry of the system while it relaxes, and any symmetry breaking in the relaxation process is spontaneous. The results of this relaxation are listed in Table V. As expected, the formation energy of the relaxed defects is substantially lower than the ideal defects. The vacancy and hexagonal interstitial were stable in all the Hamiltonians studied, and were relaxed without constraints. The tetrahedral interstitial was stable in the MS-TB and NO-TB models, but in the DF-TB model it relaxes into a split interstitial. To force the interstitial atom to remain in the tetrahedral site, the outer shell of atoms in the periodic unit cell was fixed during the relaxation. The con-

TABLE V. Formation energies for ideal point defects E_f^{ideal} and relaxation energies $\Delta E_f = E_f^{\text{relaxed}} - E_f^{\text{ideal}}$.

	DFT/LDA [a]		NO-TB		MS-TB		DF-TB	
	E_f^{ideal}	ΔE_f	E_f^{ideal}	ΔE_f	E_f^{ideal}	ΔE_f	E_f^{ideal}	ΔE_f
Tetrahedral interstitial	3.7 – 4.8	0.1 – 0.2	4.5	0.5	9.6	1.2	11.7	3.8
Hexagonal interstitial	4.3 – 5.0	0.6 – 1.1	6.3	1.3	9.7	1.2	12.9	5.2
Vacancy	3.3 – 4.3	0.4 – 0.6	4.4	1.2	6.0	0.4	3.9	0.6

[a]References 22, 26, and 27.

straint applied to this defect to keep it in the tetrahedral position accounts for the differences in the relaxed formation energy between our calculation using the DF-TB Hamiltonian and the results reported by Frauenheim *et al.*[7] Compared with all of the tight-binding Hamiltonians, previously published DFT/LDA calculations[22,26,27] generally show smaller relaxation energies for the structures considered. The difference is especially large for the tetrahedral interstitial in all of the model Hamiltonians, and in the case of the DF-TB model also for the hexagonal interstitial. The exception is the vacancy, where both the MS-TB and DF-TB models predict a relatively accurate relaxation energy (although the MS-TB model greatly overestimates both the unrelaxed and relaxed formation energies).

The NO-TB model predicts almost identical formation energies for the relaxed vacancy and tetrahedral interstitial, while the hexagonal interstitial is about 1.5 eV higher. The path connecting two tetrahedral interstitial positions through a hexagonal interstitial position would correspond to a 1.5 eV barrier. The other two model Hamiltonians predict almost identical formation energies for the two relaxed interstitials, indicating only a small energy barrier to diffusion of tetrahedral interstitials through the hexagonal configuration. These two models predict the vacancy to be 2.5 – 4.0 eV lower in energy. However, because the MS-TB and DF-TB models overestimate the formation energies of the ideal defects, they also overestimate the formation energies of the relaxed defects. In fact, the results from both of these model Hamiltonians put the formation energies of interstitials in *relaxed* configurations higher than DFT/LDA formation energies of defects in *ideal* configurations.

The geometries and symmetries of the relaxed defects are still a subject of active investigation. Accordingly, we provide here some details of the relaxed defect configurations produced by the various models considered. For the hexagonal interstitial the three Hamiltonians we studied predict an outward relaxation of the hexagonal ring and no symmetry breaking. This result is qualitatively in agreement with DFT/LDA calculations.[26] The tetrahedral interstitial is more complicated. The MS-TB Hamiltonian predicts that some of the nearest neighbors relax outward and some relax inward, producing an almost complete breaking of the symmetry of the ideal structure. The DF-TB Hamiltonian predicts outward relaxation of the neighbors to a low-symmetry structure. This low symmetry is perhaps caused by the tendency of the interstitial to relax from the tetrahedral position into a split configuration, a transition which is hindered here by the applied constraint for the reasons described above. In the NO-TB model the four neighbors of the tetrahedral interstitial relax outward. The interstitial moves towards one pair of neighboring atoms, and away from the other pair. The neighbors accommodate the distortion by completely breaking their tetrahedral symmetry. The DFT/LDA work of Kelly and Car[26] predicts a relaxed tetrahedral configuration with all of the symmetry of the ideal geometry, but the direction of the relaxation was not specified.

All four Hamiltonians predict overall inward relaxation around the vacancy in qualitative agreement with recent DFT/LDA calculations,[26,27] although they each predict a very different symmetry. The MS-TB and DF-TB Hamiltonians predict low-symmetry structures, while the NO-TB Hamiltonian predicts a structure with tetragonal symmetry, with two nonadjacent edges contracting by equal amounts, while the other four edges contract by a smaller amount. Of the three tight-binding models, only our Hamiltonian is in agreement with the DFT/LDA results of Kelly and Car[26] and Seong and Lewis,[27] which also predict a relaxation with tetragonal symmetry.

TABLE VI. Surface energies for the Si (100) and (111) surfaces. γ is the surface energy in eV per (1×1) cell; $\Delta\gamma$ is the relaxation energy relative to ideal (1×1) γ; θ is the tilt angle of dimers; d is the bond length of the dimer.

		DFT/LDA [a]	NO-TB	MS-TB	DF-TB
		Si(100)			
Ideal (1×1)	γ	2.5	1.5	2.4	1.9
Relaxed (1×1)	$\Delta\gamma$	-0.03	-0.03	-0.01	-0.01
Buckled dimer (2×1)	$\Delta\gamma$	-0.83	-0.53	-0.83	-0.62
	θ	15°	14°	12°	15°
	d (Å)	2.23	2.41	2.38	2.61
		Si(111)			
Ideal (1×1)	γ	1.56	1.19	1.67	1.24
Relaxed (1×1)	$\Delta\gamma$		-0.020	-0.003	-0.007
(2×2) T_4	$\Delta\gamma$	-0.30	-0.26	-0.17	-0.07
(2×2) H_3	$\Delta\gamma$	-0.25	-0.26	-0.17	-0.15

[a]References 28 and 29.

Finally, we have calculated the activation energies for diffusion of the various defects. The activation energy for diffusion of the vacancy is 3.5 eV (3.2 eV of formation energy and 0.3 eV of migration energy), that of the interstitial is 5.0 eV (4.0 eV of formation energy at the tetrahedral site, and 1.0 eV of migration energy through the hexagonal site) and that of the concerted exchange is 3.7 eV, including full relaxation at the saddle point (the unrelaxed saddle-point configuration with energy 5.4 eV was included in the fitting dataset).

C. Surface properties

To examine the behavior of our model Hamiltonian in an environment substantially different from the regime where it was fit, we calculated the surface energies of various low-energy reconstructions of the (100) and (111) surfaces, the two lowest-energy surfaces of silicon. Most experimental and theoretical studies of surface phenomena in silicon, including technologically relevant work such as deposition and growth, are done on one of these two surfaces.

(100) Surface: For the (100) surface we calculate the surface energy γ of the ideal surface. For each relaxed or reconstructed configuration, we compute the surface energy difference $\Delta\gamma$ relative to the ideal surface. We first relax the surface while imposing a (1×1) periodicity, which prohibits any reconstruction. We then allow the formation of symmetric dimers which eliminates one of the two dangling bonds per surface atom. When the dimerized surface is allowed to break the symmetry, a tilted dimer (2×1) reconstruction is spontaneously formed. The surface energies are listed in Table VI.

All of the Hamiltonians produce qualitatively correct results, with a stable tilted dimer (2×1) reconstruction as seen in DFT/LDA calculations[29] (shown in Fig. 2). The tilting of

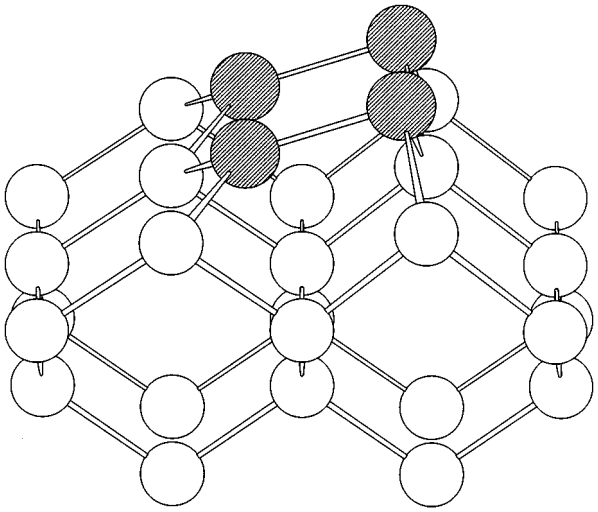

FIG. 2. (100) surface: (2×1) buckled dimer reconstruction. Surface atoms are shown shaded.

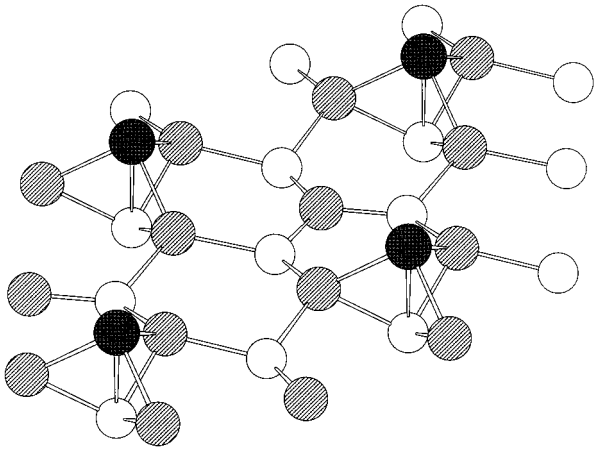

FIG. 3. (111) surface: (2×2) T_4 adatom reconstruction. Surface atoms are shown shaded, with lighter shading for those atoms that form the top layer of the ideal surface, and darker shading for the adatoms.

the dimer is caused by a Jahn-Teller distortion which raises the energy of one of the dangling bonds and lowers the energy of the other, inducing both of the unpaired electrons to go into the lower-energy dangling bond. This is a fundamentally quantum-mechanical phenomenon which all the tight-binding Hamiltonians considered here correctly reproduce. Surprisingly, some classical potentials can reproduce this feature.[1] Results from the three Hamiltonians considered are in qualitatively good agreement with each other and in agreement with DFT/LDA results. The MS-TB and DF-TB models, which predicted higher point defect formation energies, also predict higher surface energies than the NO-TB model. The accuracy of the geometrical structure of the reconstruction varies from model to model. All of the tight-binding models err in predicting a dimer bond that is longer than the equilibrium bond length, unlike DFT/LDA calculations which predict a dimer bond that is shorter than the equilibrium bond length. This bond length is determined by the balance between the large forces caused by the severe distortion of the bonds to the bulk and creation of the new bond. It is therefore sensitive to small changes in the energetics of the bond bending and formation processes. The amount of tilt of the asymmetric dimer is reproduced satisfactorily by all model Hamiltonians.

(111) Surface: The (111) surface is the cleavage plane of silicon, and the (7×7) reconstruction which minimizes its energy produces the lowest-energy (hence most stable) surface of silicon. This reconstruction has been observed experimentally and studied theoretically.[30–32] It includes features such as dimer bridges, adatoms on the surface and a stacking fault underneath half of the (7×7) cell. The stacking fault energy is very low and does not change the structure of the surface much, i.e., the faulted and unfaulted halves of the (7×7) unit cell have identical local features. The most difficult of those features to reproduce with an empirical model is the adatom geometry, which introduces significant strain to the substrate.[33] In both the faulted and unfaulted halves of the (7×7) unit cell, adatoms are arranged locally in a (2×2) configuration. For simplicity, we study the adatom geometry in a (2×2) periodicity, and in the T_4 (stable) and H_3 (metastable) positions. The ideal surface is composed of a hexagonal lattice of atoms each with one dangling bond perpendicular to the surface. The T_4 adatom reconstruction places one adatom in each (2×2) cell in the center of a triangle of surface atoms, directly above an atom of the second surface layer (shown in Fig. 3). The T_4 adatom saturates three dangling bonds on the surface with a distortion of the ideal bond angles, but introduces one more dangling bond. It can also lower its energy by forming an effective bond to the atom directly beneath it in the second surface layer. In the H_3 configuration, the adatom resides at the center of a hexagon composed of first and second layer atoms. The H_3 adatoms also saturate three dangling bonds and create a new one, but they do not have a second layer atom to bond to.

As before, we begin by calculating the ideal surface energy γ and the energy gain $\Delta\gamma$ by relaxing the surface, either with a (1×1) periodicity imposed, or with reconstructions corresponding to higher periodicity [in this case the two adatom (2×2) reconstructions]. The results are listed in Table VI.

Here the three model Hamiltonians give significantly different results. The MS-TB Hamiltonian performs reasonably well at reproducing the energy of the ideal surface, but it underestimates by a factor of two the reconstruction energies $\Delta\gamma$ of the T_4 and H_3 adatom reconstructions, and does not show an energy difference between the two. The DF-TB Hamiltonian underestimates the surface energy, and greatly underestimates the relaxation energies of the adatom reconstructions. The NO-TB Hamiltonian also underestimates the surface energy, but it is better than either of the previous tight-binding models at reproducing the relaxation energies of the adatom reconstructions. In fact, none of the tight-binding Hamiltonians predict the correct energy ordering of the reconstructions, although in all cases the adatom reconstructions are stable, which is already a significant improvement over classical potential models.[1] Continuing the trend in point defect formation energies and the (100) surface energy, the MS-TB and DF-TB models predict higher energies for the (111) surface than the NO-TB model.

IV. DISCUSSION

The two Hamiltonians that we compare to our current work, those of Menon and Subbaswamy[6] and Frauenheim *et al.*,[7] are both nonorthogonal tight-binding Hamiltonians with a minimal sp^3 basis in the two-center approximation. The functional forms of their matrix elements are derived in very different ways. The MS-TB model uses a very simple functional form and the assumptions of an extended Hückel theory to keep the number of parameters to a minimum. Most of its parameters are taken directly from Harrison's work.[9] Only three parameters are left to be fit to experimental data. The DF-TB model uses direct calculations of the matrix elements from DFT/LDA single-atom contracted wave functions. Only the classical repulsion term is fit to experimental data. Despite the differences in the functional forms of these two Hamiltonians, they share some favorable and unfavorable features. Both reproduce the energetics of the bulk diamond structure fairly well, and both provide a reasonable description of the low-energy surface reconstructions we have considered. However, neither reproduces well the cohesive energy curves of the other low-energy bulk structures of silicon. Both of these model Hamiltonians overestimate the formation energies of point defects, and both overestimate the band gap of the diamond structure.

It appears from our observations that the band gap and the point defect formation energies are linked. In the fitting process we attempted to reduce the predicted formation energies of the point defects, while maintaining an accurate band gap. We found that whenever the defect formation energies decrease, so does the band gap. The behavior of the MS-TB and DF-TB models is consistent with this observation. Both have substantially larger band gaps than the NO-TB model, and both greatly overestimate the formation energies of the point defects we have considered. A related observation is that these models also predict higher surface energies than the NO-TB model.

The defect formation energies are still overestimated by the model we have introduced, despite the fact that we include these energies in the fitting dataset. To get more accurate defect formation energies, the constraint on the band gap can be relaxed, but the gap then becomes much smaller than the experimental value. We have chosen a compromise between accurate defect formation energies and a qualitatively correct band structure.

The task of producing tight-binding Hamiltonians for silicon is a challenging one. Previously presented models have not been fit to geometries that are similar to those of defects in crystalline silicon and to amorphous silicon, and their applicability to these systems cannot be taken for granted. Our model Hamiltonian gives good agreement with DFT/LDA calculations for total energies of geometries relevant to extended silicon structures. It predicts accurately bulk properties such as the energetics of experimentally relevant crystal phases and the elastic constants of the diamond crystal structure. It also reproduces the energetics of distorted (but still experimentally relevant) geometries such as point defects and surfaces. It is hoped that this Hamiltonian can contribute to advances in accurate simulations of large scale systems and complex processes in crystalline and amorphous silicon.

ACKNOWLEDGMENT

This work was supported by Harvard's Materials Research Science and Engineering Center, which is funded by NSF through Grant No. DMR-99-00396.

[1] For a recent review see H. Balamane, T. Halicioglu, and W. A. Tiller, Phys. Rev. B **46**, 2250 (1992), and references therein.
[2] A. P. Sutton, M. W. Finnis, D. G. Pettifor, and Y. Ohta, J. Phys. C **21**, 35 (1988); L. Goodwin, A. J. Skinner, and D. G. Pettifor, Europhys. Lett. **9**, 701 (1989).
[3] C. Z. Wang, K. M. Ho, and C. T. Chan, Phys. Rev. Lett. **70**, 611 (1993).
[4] J. L. Mercer, Jr. and M. Y. Chou, Phys. Rev. B **49**, 8506 (1994).
[5] I. Kwon, R. Biswas, C. Z. Wang, K. M. Ho, and C. M. Soukoulis, Phys. Rev. B **49**, 7242 (1994).
[6] M. Menon and K. R. Subbaswamy, Phys. Rev. B **47**, 12754 (1993); **50**, 11577 (1994).
[7] P. Blaudeck, Th. Frauenheim, D. Porezag, G. Seifert, and E. Fromm, J. Phys.: Condens. Matter **C4**, 6389 (1992); Th. Frauenheim, F. Weich, Th. Köhler, S. Uhlmann, D. Porezag, and G. Seifert, Phys. Rev. B **52**, 11492 (1995).
[8] N. Bernstein and E. Kaxiras, in *Materials Theory, Simulations, and Parallel Algorithms*, edited by E. Kaxiras, J. Joannopoulos, P. Vashishta, and R. Kalia, MRS Symposia Proceedings No. 408 (Materials Research Society, Pittsburgh, 1996), p. 55.
[9] W. A. Harrison, *Electronic Structure and the Properties of Solids* (Freeman, San Francisco, 1980).
[10] K. C. Pandey, Phys. Rev. Lett. **57**, 2287 (1986).
[11] S. M. Hu, Mater. Sci. Eng. R. Rep. **R13**, 105 (1994); **R13,** 185 (1994), and references therein.
[12] J. C. Jamieson, Science **139**, 762 (1963).
[13] M. I. McMahon and R. J. Nelmes, Phys. Rev. B **47**, 8337 (1993), and references therein.
[14] M. T. Yin and M. L. Cohen, Phys. Rev. B **26**, 5668 (1982).
[15] L. L. Boyer, E. Kaxiras, J. L. Feldman, J. Q. Broughton, and M. J. Mehl, Phys. Rev. Lett. **67**, 715 (1991).
[16] N. Moll, M. Bockstedte, M. Fuchs, E. Pehlke, and M. Scheffler, Phys. Rev. B **52**, 2550 (1995).
[17] F. D. Murnaghan, Proc. Natl. Acad. Sci. USA **30**, 244 (1944).
[18] O. H. Nielsen and R. M. Martin, Phys. Rev. B **32**, 3792 (1985).
[19] A. Fukumoto, Phys. Rev. B **42**, 7462 (1990).
[20] G. A. Baraff and M. Schlüter, Phys. Rev. B **30**, 3460 (1984).
[21] V. Fiorentini and A. Baldereschi, Phys. Rev. B **51**, 17 196 (1995).
[22] Y. Bar-Yam and J. D. Joannopoulos, Phys. Rev. Lett. **52**, 1129 (1984).
[23] M. Nastar, V. V. Bulatov, and S. Yip, Phys. Rev. B **53**, 13 521 (1996).
[24] S. T. Pantelides, Phys. Rev. Lett. **57**, 2979 (1986).
[25] S. Roorda, W. C. Sinke, J. M. Poate, D. C. Jacobson, S. Dierker, B. S. Dennis, D. J. Eaglesham, F. Spaepen, and P. Fuoss, Phys. Rev. B **44**, 3702 (1991).
[26] P. J. Kelly and R. Car, Phys. Rev. B **45**, 6543 (1992).
[27] H. Seong and L. J. Lewis, Phys. Rev. B **53**, 9791 (1996).
[28] I. P. Batra, Phys. Rev. B **41**, 5048 (1990).

[29] J. D abrowksi and M. Scheffler, Appl. Surf. Sci. **56-58**, 15 (1992).
[30] G. Binnig, H. Rohrer, Ch. Gerber, and E. Weibel, Phys. Rev. Lett. **50**, 120 (1983).
[31] K. Takayanagi, Y. Tanishiro, M. Takahashi, and S. Takahashi, J. Vac. Sci. Technol. A **3**, 1502 (1985).
[32] J. E. Northrup, Phys. Rev. Lett. **57**, 154 (1986).
[33] I.-W. Lyo, E. Kaxiras, and Ph. Avouris, Phys. Rev. Lett. **63**, 1261 (1989).